The Electron Momentum Distribution in Lead *

D. N. Timms

Department of Applied Physics and Physical Electronics, Portsmouth Polytechnic, Portsmouth PO1 2DZ, UK

M. J. Cooper

Department of Physics, University of Warwick, Coventry CV4 7AL, UK

Z. Naturforsch. **48a**, 343 – 347 (1993); received January 11, 1992

Directional Compton profiles have been measured along the [100], [110] and [111] crystallographic axes in lead using 412 and 59.5 keV γ-radiation from ^{198}Au and ^{241}Am radioisotope sources, respectively. Both measurements are in mutual agreement and show a small anisotropy, which is just distinguishable within the statistical error. The spherically averaged data have been compared with the predictions of relativistic Hartree-Fock (RHF) and non-relativistic Hartree-Fock (HF) free atom calculations. As expected, the experiment clearly favours the RHF rather than the HF calculation.

Key words: Compton profile; Electron momentum distribution; Relative effects; Lead.

1. Introduction

The Compton profile is deduced from the measured x-ray or γ-ray double-differential scattering cross-section and is the projection of the electron momentum density, $n(\boldsymbol{p})$ along the scattering vector, usually chosen as the z-axis of a Cartesian coordinate system (see [1])

$$J(p_z) = \iint n(\boldsymbol{p})\, \mathrm{d}p_x \mathrm{d}p_y \,. \tag{1}$$

The Compton profile is subject to the normalisation rule

$$\int_{-\infty}^{+\infty} J(p_z)\, \mathrm{d}p_z = Z \,, \tag{2}$$

where Z is the atomic number of the scatterer.

The Compton profile line shape is very sensitive to the behaviour of the valence electrons and thus provides a basis to test band theory electron wave functions. After suitable normalisation, Compton data are compared directly with theoretical predictions for $J(p_z)$ and are also interpreted in terms of differences between pairs of directional profiles, i.e.

$$\Delta J(p_z) = J_{hkl}(p_z) - J_{h'k'l'}(p_z) \,, \tag{3}$$

where hkl and $h'k'l'$ denote planes perpendicular to the scattering vector. The latter approach eliminates or at least minimises residual systematic errors after data processing and also removes the isotropic core contribution from $J(p_z)$.

Relativistic Hartree-Fock (RHF) Compton profile calculations of heavy elements [2–4] have demonstrated that the "relativistic effects" are not limited to electrons situated near to the nucleus. The relativistic spatial wave functions of the rapidly moving electrons in the inner orbitals are pulled in towards the nucleus when compared with non-relativistic Hartree-Fock (HF) wave functions as its mass increases, [5]. This relativistic contraction of the core electron distribution leads to a more effective screening of the nuclear charge.

The more sharply peaked position-space wave function of the core electron leads to a more delocalised momentum-space wave function and thus a flatter core electron momentum-space wave function. The consequence is that the Compton profile derived from a relativistic model is broader than the corresponding profile derived from a non-relativistic model. We expect a relativistic model to better predict the behaviour of the tightly bound innermost 1 s, 2 s and 2 p-orbitals of heavy elements. However, since the single-particle electron wave functions must be orthogonal, the outer s and p orbitals must also be affected by the relativistic nature of the core electrons. The importance of relativistic modelling in heavy metals is emphasised in a first-principles calculation of the crystal structure of

* Presented at the Sagamore X Conference on Charge, Spin and Momentum Densities, Konstanz, Fed. Rep. of Germany, September 1–7, 1991.

Reprint requests to Dr. David N. Timms, Applied Physics and Physical Electronics Department, Portsmouth Polytechnic, Park Building, King Henry I St., Portsmouth, PO1 2DZ, United Kingdom.

0932-0784 / 93 / 0100-0343 $ 01.30/0. – Please order a reprint rather than making your own copy.

lead [6] where a non-relativistic model resulted in the diamond structure of lead being more stable than the observed face-centred cubic structure.

A measure of the relativistic flattening of $J(p_z)$ is provided by the quantity $(J_{\mathrm{RHF}}(p_z) - J_{\mathrm{HF}}(p_z))/J_{\mathrm{HF}}(p_z)$ at $J(0)$. Mendelsohn et al. [3] cite the following results: argon ($Z=18$) 0.187%, krypton ($Z=36$) 0.712% and lead ($Z=82$) 5.24%. As expected the effect is more significant for heavy elements.

In an earlier Compton study [7], ^{123m}Te γ-radiation was used to measure the Compton profiles of the rare gases Ar and Kr, and the results were compared with relativistic and non-relativistic calculations of $J(p_z)$. The relativistic flattening of $J(p_z)$ in these gases is small, and within the statistical accuracy of the results it was not possible to distinguish between the two calculations. The effects of relativistic flattening in lead have been previously investigated [8] although the experimental results were of poor statistical accuracy ($\pm 4\%$ $J(0)$), low signal-to-noise ratio and contained a large multiple-scattering contribution ($> 20\%$ of the total intensity). However, the results did favour the RHF calculation of $J(p_z)$ for lead.

Heller and Moreira [9] have deduced the Compton profiles of lead (and aluminium) from measurements with ^{137}Cs γ-radiation (662 keV). They determined continuous single-scattering Compton profiles for each electron orbital from the discrete values of $J(p_z)$ given in [3]. The differential scattering cross-section was calculated using a Monte Carlo method to simulate the theoretical γ-ray spectra characterised by the particular scattering angle and scattered energy used. Good agreement between experiment and simulation was observed only when the Ribberfors expressions [10, 11] for scattering through angles differing from 180 degrees were employed. This work strongly supported the relativistic cross-section derived by Ribberfors [10, 11].

Pattison and Schneider [12] used 412 keV γ-radiation to measure the Compton profiles of lead and gold up to momentum values of 110 a.u. (1 a.u. of momentum $= 1.99 \cdot 10^{-24}$ m kg s^{-1}). They limited their interpretation to the momentum range 60–110 a.u. where the profile line shape is dominated by the behaviour of the relativistic core electrons. The K- and L-shell binding edges contained within this momentum region were clearly resolved in this experiment and well modelled by an RHF calculation of $J(p_z)$. As with [9] the good agreement observed supported strongly the relativistic cross-section derived by Ribberfors [10, 11].

The objectives of the present study were twofold. The first was to deduce accurate directional Compton profiles of lead to encourage a theoretical band structure calculation for lead. The second was to illustrate the fact that non-relativistic theories are inadequate for modelling the electron momentum density and Compton profiles of lead.

2. Measurements and Data Analysis

The [100], [110] and [111] directional Compton profiles of lead were deduced from Compton scattering measurements on single-crystal slices at γ-ray energies of 412 and 59.5 keV. The high-energy measurements were made using the ^{198}Au Compton spectrometer [13] that is sited at the Rutherford Appleton Laboratory. The ^{198}Au source has a useful lifetime of about 10 days (the initial activity is 150–200 Ci and the ^{198}Au isotope has a half life of 2.7 days). A new source was used to measure each directional profile. The lower-energy, lower-resolution measurements were undertaken at the University of Warwick using the ^{241}Am spectrometer [14]. More than thirty days were required for each directional measurement with the 5 Ci ^{241}Am source, which has a half life of 452 years.

The individual oriented single-crystal discs, diameter 15.0 ± 0.1 mm, were cut from a large cylindrical single-crystal bar and reduced to a common thickness (1.60 ± 0.05 mm) using spark erosion techniques. The samples were then etched to remove surface damage. Individual energy spectra were accumulated over a period of 260 hours (412 keV) and 400 hours (59.5 keV), enabled integrated counts of approximately 6×10^6 and 3×10^6 to be recorded in the respective Compton profiles. Low count rates (~ 5 cps under the Compton profile) were observed: this is a direct consequence of the high photoelectric absorption cross-section of lead.

The data were processed by application of a series of energy-dependent corrections, which were applied according to a well-tested scheme detailed in [15]. The detector response function, the energy dependence of the detector efficiency, the source-dependent and independent background corrections and the contribution from multiple scattering were all closely scrutinised. For the high-energy data the source-independent background or static background contribution was established to be 65% of the integrated total background and was removed using the procedure outlined in [16].

As usual, a Monte Carlo simulation [17] was employed to determine the energy distribution of the multiple scattering. For the high and low-energy spectrometers the contributions from multiple scattering were 13.5% and 3.7% of $J(p_z)$, respectively. These percentages are small compared with Compton measurements on lighter materials [18, 19] and are a further consequence of the large photoelectric absorption cross-section of lead. It was assumed that the multiple-scattering profile had no directional dependence, and the constant sample thickness ensured that the same correction could be applied to each directional profile.

After application of the data processing routines the high-energy data were normalised to the free-atom value of 29.226 electrons over the momentum range 0 to 7 a.u. The K, L, and M electron-shell binding energies of lead are 88.01 keV, 30–15.9 keV, and 2.5–3.8 keV, respectively. Hence in the low-energy experiment it was not possible to excite the 1s electrons in lead with 59.5 keV radiation and the 2s and 2p-electrons did not contribute for momentum values greater than −7 a.u. and +11 a.u., respectively. The binding edges were acounted for in the normalisation of the low-energy data.

3. Discussion

The experimental directional Compton profiles measured with 412 keV γ-radiation and the isotropic RHF [3, 4] and HF [5] theoretical profiles are listed in Table 1. Both theoretical profiles have been convoluted with Gaussians of FWHM = 0.4 a.u. in order to match the experimental resolution half width. The difficulties encountered in removing the systematic errors from $J(p_z)$ in the ^{241}Am experiment (see [18, 19, 15]), together with the breakdown of the impulse approximation for the K, L, and M-electrons, lead to the conclusion that symmetric profiles will not be forthcoming from these data. For this reason the low-energy data were used only to confirm the anisotropy measured with the ^{198}Au spectrometer.

Figure 1 shows the differences between directional profiles of lead obtained from measurements with 412 keV and 59.5 keV γ-radiation. As the core electron contribution to the profile is isotropic, the observed anisotropy in $J(p_z)$ gives a measure of the anisotropy in the valence electron momentum density. Taking into account the poorer quality of the low-energy data (i.e. ±0.62% $J(0)$) compared with that of the high-energy data (±0.39% $J(0)$), it can be seen that both data sets are in mutual agreement.

Table 1. The experimental and theoretical Compton profiles of lead along the [100], [110], and [111] crystallographic directions. The experimental data were obtained from measurements with 412 keV γ-radiation. The RHF and HF free-atom profiles are taken from [3, 4] and [5], respectively. Both theoretical profiles have been convoluted with a Gaussian of 0.4 a.u. FWHM to mimic the experimental resolution half width of the ^{198}Au spectrometer.

p_z	Experiment [100]	Experiment [110]	Experiment [111]	Relativistic free atom	Nonrelativistic free atom
0.0	10.252 ±0.040	10.095	10.141	10.980	11.470
0.1	10.177	10.018	10.169	10.881	11.346
0.2	10.064	9.869	10.100	10.598	10.991
0.3	9.837	9.684	9.897	10.175	10.461
0.4	9.519	9.443	9.620	9.669	9.839
0.5	9.218	9.062	9.259	9.140	9.213
0.6	8.773	8.653	8.825	8.637	8.650
0.7	8.281	8.293	8.310	8.193	8.181
0.8	7.862	7.886	7.839	7.820	7.809
0.9	7.471	7.479	7.449	7.510	7.512
1.0	7.148	7.109	7.123	7.248	7.265
1.2	6.683	6.687	6.639	6.799	6.833
1.4	6.221	6.209	6.239	6.370	6.409
1.6	5.846	5.887	5.845	5.926	5.966
1.8	5.400	5.370	5.403	5.476	5.513
2.0	5.025	5.055	4.973	5.043	5.077
2.5	4.053	4.082	4.129	4.130	4.185
3.0	3.489 ±0.031	3.474	3.506	3.513	3.569
4.0	2.843	2.844	2.847	2.842	2.852
5.0	2.484	2.484	2.487	2.399	2.377
6.0	2.085	2.099	2.085	1.980	1.990
7.0	1.737	1.770	1.715	1.718	1.744

The results show that lead exhibits only a small anisotropy (~1% $J(0)$), which is just statistically significant. Although the anisotropies are small, they appear to be associated with the [111]-direction and correspond to a shift of electron density from the region 0.75 a.u. $< p_z <$ 1.5 a.u. to the region $p_z <$ 0.75 a.u. The Brillouin zone boundary in the [111]-direction is at 0.6 a.u. Although the density of states and the Fermi surface of lead have been calculated by a number of workers (see, for example, [20–23]), it is difficult to draw any direct comparisons between their work and these data.

A relativistic Compton profile will have a larger second moment (i.e. greater kinetic energy) than the corresponding non-relativistic profile, and by the virial theorem this corresponds to a lower total energy. The kinetic-energy difference will not be visible in $J(p_z)$ at high momentum, where a large change in the second

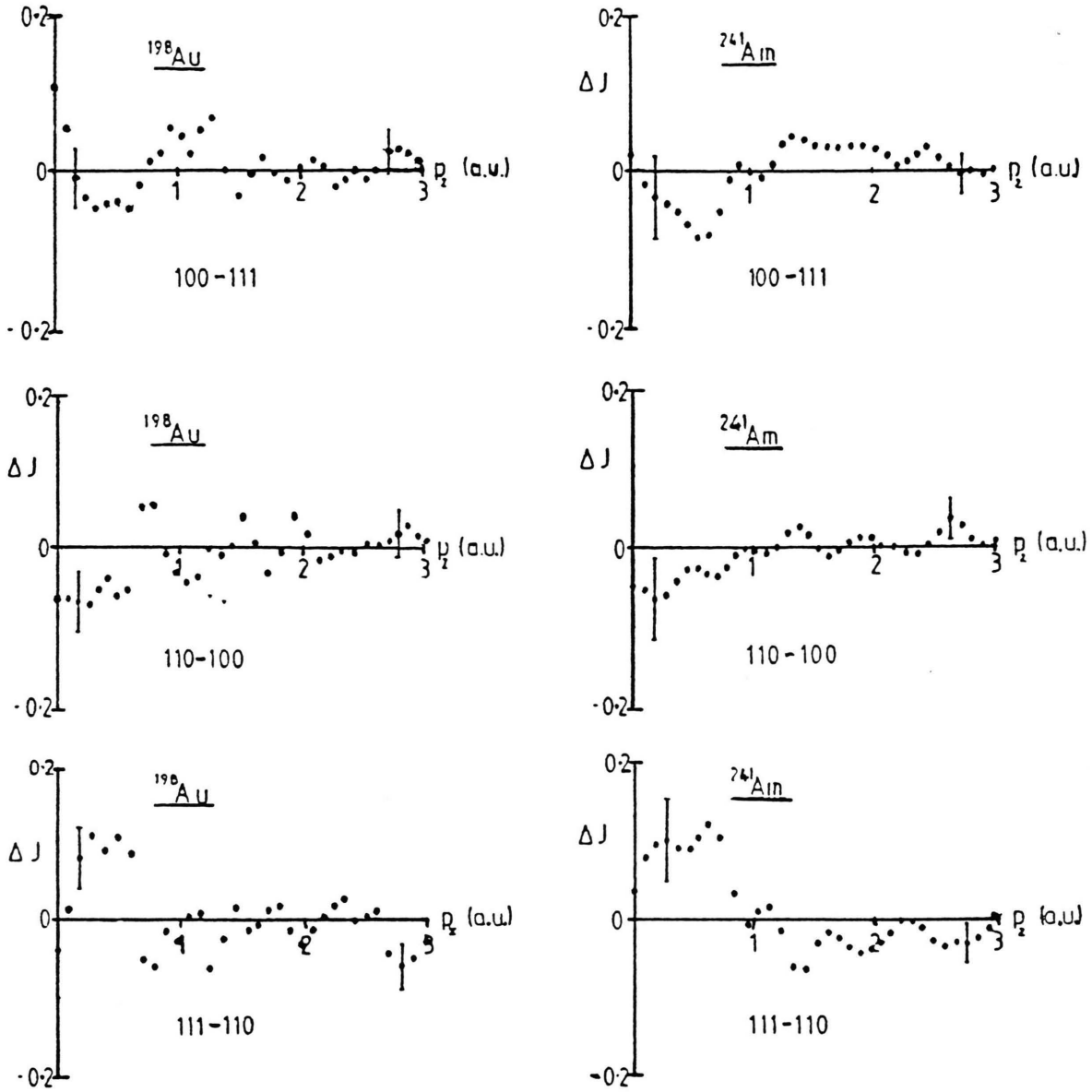

Fig. 1. The Compton profile anisotropies of lead measured with 412 keV and 59.5 keV γ-radiation. The data have been normalised to the free-atom value in the momentum range shown.

moment of $J(p_z)$ will result in only a small change in the magnitude of $J(p_z)$. This is illustrated by the fact that theoretical profiles listed in Table 1 are within $\sim 1\%$ of each other at $p_z > 3$ a.u.

Figure 2 shows the difference between a spherically averaged experimental profile formed from a weighted average of the data and the theoretical profiles. The experiment clearly favours the relativistic calculation at low momentum. The relativistic flattening of the momentum distribution is evident here as a shift of electron density from the low-momentum region, $p_z < 0.4$ a.u., to the region 0.4 a.u. $< p_z < 1.0$ a.u. The relativistic free-atom model is not able to account for solid-state effects in lead and as a result still overestimates by $\sim 7\%$ $J(0)$ the contribution from the bound electrons to $J(p_z)$ at low momentum. It is apparent from Fig. 2 that the experiment does not reduce exactly to either free-atom profile at high momentum.

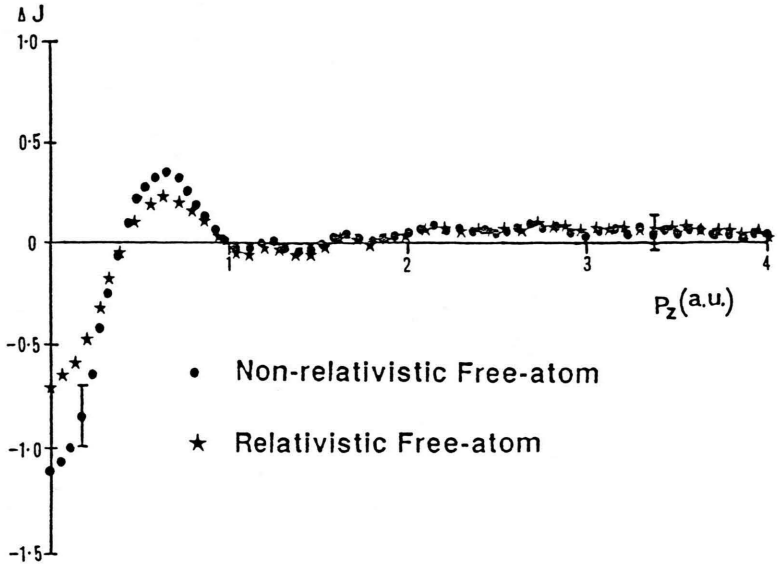

Fig. 2. The difference between the spherically averaged, experimental Compton profile of lead measured with 412 keV γ-radiation and the HF and RHF Compton profiles of lead.

This discrepancy, which is of the order of 1%$J(0)$, may be attributed to residual systematic errors remaining in the data after data processing.

4. Conclusions

The large observed discrepancies between the experimental data and both free-atom theories illustrate most strongly the inadequacy of these calculations to model the electron momentum density in lead. The consequence is that only a qualitative interpretation of the experimental data is possible at this time, and a relativistic band structure calculation of the electron momentum density and Compton profiles of lead is required if a quantitative interpretation of these data is to be made. Kubo and Yamashita [20] have already calculated a self-consistent relativistic band structure of lead at normal and high pressure using the symmetrised relativistic APW method, and it is hoped that this work will encourage such a relativistic band structure calculation of the Compton profiles of lead.

Acknowledgements

The experimental work forms part of a programme of Compton scattering research work supported by the SERC in the United Kingdom.

[1] M. J. Cooper, Rep. Prog. Phys. **48,** 415 (1985).
[2] L. B. Mendelsohn and E. A. Biggs, U.S. Atomic Energy Conf. 720404, **3,** 1142 (1973).
[3] L. B. Mendelsohn, F. Biggs, and J. B. Mann, Chem. Phys. Lett. **26,** 521 (1974).
[4] F. Biggs, L. B. Mendelsohn, and J. B. Mann, Atomic and Nuclear Data Tables **16,** 201 (1975).
[5] J. B. Mann, Structure Calc. II, Report LA-3691, Los Alamos Sci. Lab. 1968.
[6] N. E. Christensen, S. Satpathy, and Z. Pawlowska, Phys. Rev. B **34,** 5977 (1986).
[7] P. Eisenberger and W. A. Reed, Phys. Rev. A **2,** 415 (1972).
[8] R. S. Holt, PhD thesis 1979, University of Warwick, England.
[9] M. V. Heller and J. R. Moreira, Phys. Rev. B **31,** 4146 (1985).
[10] R. Ribberfors, Phys. Rev. B **12,** 2067 (1975).
[11] R. Ribberfors, Phys. Rev. B **12,** 3136 (1975).
[12] P. Pattison and J. R. Schneider, J. Phys. B **12,** 4013 (1979).
[13] R. S. Holt, M. J. Cooper, J. L. DuBard, J. B. Forsyth, T. L. Jones, and K. Knights, J. Phys. E **12,** 1148 (1979).
[14] M. J. Cooper, R. S. Holt, and J. L. DuBard, J. Phys. E: Sci. Instrum. **11,** 1145 (1978).
[15] D. N. Timms, PhD thesis 1989, University of Warwick, England.
[16] D. N. Timms, M. J. Cooper, R. S. Holt, F. Itoh, T. Kobayashi, and H. Nara, J. Phys.: Conden. Matter **2,** 10517 (1990).
[17] J. Felsteiner, P. Pattison, and M. J. Cooper, Phil. Mag. B **54,** 537 (1974).
[18] D. A. Cardwell and M. J. Cooper, Phil. Mag. B **54,** 37 (1986).
[19] D. A. Cardwell, J. M. Cooper, and S. Wakoh, J. Phys..: Conden. Matter **1,** 541 (1989).
[20] Y. Kubo and J. Yamashita, J. Phys. F **16,** 2017 (1986).
[21] T. L. Loucks, Phys. Rev. Lett. **14,** 1072 (1965).
[22] F. R. McFeely, L. Fey, S. P. Kowalczyk, and D. A. Shirly, Sol. State Comm. **17,** 1415 (1975).
[23] A. D. Zdetsis, D. A. Papaconstantopoulos, and E. N. Economou, J. Phys. F.: Met. Phys. **10,** 1149 (1980).